AIP | Review of Scientific Instruments

Thermal conductivity measurements of non-metals via combined time- and frequency-domain thermoreflectance without a metal film transducer

L. Wang, R. Cheaito, J. L. Braun, A. Giri, and P. E. Hopkins

Citation: Review of Scientific Instruments **87**, 094902 (2016); doi: 10.1063/1.4962711
View online: http://dx.doi.org/10.1063/1.4962711
View Table of Contents: http://scitation.aip.org/content/aip/journal/rsi/87/9?ver=pdfcov
Published by the AIP Publishing

Thermal conductivity measurements of non-metals via combined time- and frequency-domain thermoreflectance without a metal film transducer

L. Wang, R. Cheaito, J. L. Braun, A. Giri, and P. E. Hopkins
Department of Mechanical and Aerospace Engineering, University of Virginia, Charlottesville, Virginia 22904, USA

(Received 18 July 2016; accepted 30 August 2016; published online 22 September 2016)

The thermoreflectance-based techniques time- and frequency-domain thermoreflectance (TDTR and FDTR, respectively) have emerged as robust platforms to measure the thermophysical properties of a wide array of systems on varying length scales. Routine in the implementation of these techniques is the application of a thin metal film on the surface of the sample of interest to serve as an opto-thermal transducer ensuring the measured modulated reflectivity is dominated by the change in thermoreflectance of the sample. Here, we outline a method to directly measure the thermal conductivities of bulk materials without using a metal transducer layer using a standard TDTR/FDTR experiment. A major key in this approach is the use of a thermal model with z-dependent heat source when the optical penetration depth is comparable to the beam sizes and measuring the FDTR response at a long delay time to minimize non-thermoreflectivity contributions to the modulated reflectance signals (such as free carrier excitations). Using this approach, we demonstrate the ability to measure the thermal conductivity on three semiconductors, intrinsic Si (100), GaAs (100), and InSb (100), the results of which are validated with FDTR measurements on the same wafers with aluminum transducers. We outline the major sources of uncertainty in this approach, including frequency dependent heating and precise knowledge of the pump and probe spot sizes. As a result, we discuss appropriate pump-frequency ranges in which to implement this TDTR/FDTR approach and present a procedure to measure the effective spot sizes by fitting the FDTR data of an 80 nm Al/SiO_2 sample at a time delay in which the spot size sensitivity dominates an FDTR measurement over the substrate thermal properties. Our method provides a more convenient way to directly measure the thermal conductivities of semiconductors. *Published by AIP Publishing.* [http://dx.doi.org/10.1063/1.4962711]

I. INTRODUCTION

Thermoreflectance-based techniques,[1–4] such as time- and frequency-domain thermoreflectance (TDTR[5] and FDTR,[6] respectively), have emerged as powerful thermometry platforms to measure and interrogate the thermal properties of a wide range of bulk materials and nanosystems.[7–9] For example, TDTR and/or FDTR have been used to measure the thermal conductivity of bulk solids,[6,10,11] exceptionally low thermal conductivity thin films,[12–17] vibrational heat capacity,[17–19] and thermal transport properties of nanocomposites, such as superlattices,[20–24] alloys and nanowire matrices,[25–27] and the thermal boundary conductance across material interfaces,[28] including structurally/compositionally varying interfaces,[29–37] interfaces adjacent to low dimensional structures (e.g., self-assembled monolayers and graphene),[38–42] and solid/liquid interfaces.[43–46] Iterations of these TDTR and/or FDTR techniques have demonstrated potential promise to go beyond thermal property measurements of systems, and gain insight into the vibrational mean free path spectra of solids (relating to the "thermal conductivity accumulation function"),[47–55] the spectral coupling of phonons across interfaces (relating to the "thermal boundary conductance accumulation function"),[10] and the spatial variation of thermal conductivity in composite systems (resulting in spatial "mapping" of the thermal conductivity with micron resolution).[56–58]

Thermoreflectance techniques, by definition, rely on the principle of thermoreflectance in their metrologies.[1,59–61] Stated differently, the measurements of thermal properties using TDTR or FDTR rely on a material's change in reflectivity due to the change in its temperature. More specifically, these pump-probe metrologies embrace thermomodulation reflectivity in which a small oscillating temperature rise is induced at some frequency caused by a modulated pump beam, while the reflectivity is monitored with the probe beam through electronic detection that is synced to the pump modulation to measure the change in reflectivity at this frequency. Hence, the most fundamental assumption of TDTR and FDTR for use as a metrology of strictly thermal transport properties is that the measured reflectivity of the probe is related to the temperature change induced by the modulated pump pulses.

Due to this fundamental necessity, it is common practice to deposit a thin metal film on the surface of any material system to be measured with TDTR and/or FDTR in order to relate the optical reflectivity to a temperature change,[7,62] and thereby relate this measured reflectivity to the thermal properties of interest. This ensures that the thermoreflectivity can be directly and linearly related to the temperature change, since the primary component driving the reflectivity in metals is the electronic distribution, which is mainly related to the temperature of the material (assuming relatively small electron-phonon nonequilibrium—which can lead to

nonlinear reflectivities[59,60,63]—and relatively small strain—which can lead to changes in the piezoreflectance coefficient that will also impact the changes in reflectivity).[64–66] This is unlike non-metals where not only temperature but also conduction band carrier population can change the reflectivity,[67–69] and therefore, the pump excitation in a TDTR and/or FDTR measurement will change both of these components to the modulated reflectivity (i.e., both the thermo- and carrier-reflectivity contributions in the measured signal).

However, the advantage of using a metal film as a thermoreflectivity transducer goes beyond just this optical-thermal transduction. This configuration ensures a relatively small optical penetration depth (on the order of ~10–20 nm for most metals over a wide swath of near-UV, visible, and IR wavelengths),[70] validating the assumption of a surface heating event, which facilitates traditionally used models for modulated heat transfer in composite media.[5,71–74] Furthermore, due to the relatively fast equilibration of electrons into a Fermi distribution and with the lattice,[75–77] a single temperature on the surface of the metal-coated sample can be assumed.

Taken together, the advantages of using a metal film in TDTR and/or FDTR measurements lie in:

(i) near surface optical absorption;
(ii) direct relationship between reflectivity change and temperature change (i.e., nearly entirely thermoreflectance dominated signal);
(iii) single temperature assumption among excited states.

Addressing assumption (i), recent work by Yang *et al.*[78] incorporated a finite pump and probe penetration depth into FDTR analysis and demonstrated the ability to implement this model in thermal conductivity measurements of amorphous silicon coated SiO_2 and Si by fitting the thermal conductivity of the amorphous silicon and the combined optical penetration depth of the pump and probe. This advancement demonstrates promise in the quest for wider implementation of FDTR, but still is limited in the fact that (ii) and (iii) must be assumed, which is strongly dependent on the material system of interest; furthermore, the approach of Yang *et al.*[78] exemplifies the fitting of both the thermal property of interest and the combined penetration depth. As we demonstrate in this work, for bulk systems, the sensitivities of FDTR measurements to the optical and energy penetration depths and the thermal conductivity can be of similar magnitudes, thereby increasing measurement uncertainties if both quantities are simultaneously fit.

Assumptions (ii) and (iii) are relatively similar when considering non-metals, and these were addressed previously by Hurley *et al.*[79] and Khafizov *et al.*[80] for pump-probe time domain thermoreflectivity-based measurements with pulsed lasers. In these works, the authors used a time-domain approach (as opposed to the strictly frequency domain demonstration of Yang *et al.*[78]) with spatially varying offset pump and probe beams to measure the thermal conductivity of various silicon samples by directly probing the silicon without a metal transducer. Their approach analyzed the thermoreflectivity data at time scales after electronic recombination occurred in their silicon samples, thereby validating assumption (iii) (nonequilibrium), and ensuring that the measured change in reflectivity in silicon was dominated by the temperature change and not the excited carrier distribution (since the carriers had recombined), thereby validating assumption (ii). These works enhanced recombination on the surface of their Si samples by mechanically roughening the surface.

Even taking into account these previous advances of TDTR or FDTR in Refs. 78–80, there still lacks a standard approach to measure the thermal conductivity of solids using TDTR and/or FDTR without the use of a metal film transducer, as some combination of assumptions (i)–(iii) must be applied via either modification to the sample, which is not ideal for nondestructive evaluation, or fitting for the absorption profile, which can lead to decreased sensitivities (increased uncertainties) in thermophysical property determination. In response, our present work details a metrology to directly measure the thermal conductivity of non-metallic systems through a combined TDTR/FDTR method (FDTR at judiciously chosen pump-probe delay times) without the use of a metal film transducer. A major advance in this approach is the ability to use TDTR in its standardized and well-adopted configuration[5] to choose delay times in which the majority of electronic recombination has occurred, thereby ensuring that the measured change in reflectivity is dominated by the thermoreflectance and not the change in carrier density or strain. We identify this thermoreflectance dominated delay time via examination of the in-phase component of our TDTR signal using different pump and probe powers, with additional theoretical considerations of carrier effects on the change in reflectivity described in Section III. Furthermore, we establish a rule-of-thumb that can be checked using the standard TDTR/FDTR configuration to ensure that measurements are conducted in the thermal-dominated regime (as opposed to the carrier regime), a procedure for which has been established in the transient thermal grating technique;[81–83] note, the transient thermal grating technique has demonstrated the ability to measure in-plane thermal conductivity of materials without the use of a metal layer.[81,82]

Following the identification of the thermoreflectance-dominated delay time, we then analyze the FDTR signal at this set time, allowing for standard TDTR/FDTR analyses to be applied (i.e., the use of the out-of-phase signal and the ratio of the in-phase to out-of-phase signals), regardless of the lack of a metal transducer. To permit this approach, we derive a thermal model with a z-dependent heat source and probe depth that is used to fit the experimental data in order to extract the thermal conductivities; we do not fit for these depths and use literature values thereby ensuring maximal sensitivity (minimal uncertainty) in our thermal conductivity fits, which is the only fitting parameter applied to our non-metallic systems using this approach.

Our paper is organized as follows: first, we describe our TDTR/FDTR experimental setup. Second, we present a detailed discussion of this technique, including carrier and thermoreflectivity calculations, the thermal model, and the delay times to which we fit the FDTR data, along with the frequency range to perform these FDTR measurements. We then present our FDTR results on bulk Si, GaAs, and InSb wafers and compare the results with the thermal conductivities measured on the same semiconductor wafers with a thin

aluminum transducer layer deposited on top. Finally, we perform a sensitivity analysis and discuss the potential sources of error that should be taken into account, which identifies the limitations of this method.

II. EXPERIMENTAL SETUP

In this work, we develop the methodology to measure the thermal conductivity of silicon (100), GaAs (100), and InSb (100) wafers using our combined TDTR/FDTR approach without the use of a metal transducer; we purchased the GaAs (100) wafers from two different vendors: UniversityWafer and MTI Corporation. For comparison, we also deposited ~80 nm Al film (precise thicknesses verified with picosecond acoustics and mechanical profilometry)[64–66] on the same semiconductor wafers with electron beam evaporation and measured the thermal conductivities with FDTR. Our various TDTR/FDTR measurements described in this work are performed using a typical optical pump-probe thermometry experiment[2–4,84] in a nearly identical geometry to the now standardized, well-adopted TDTR configuration.[5] A mode-locked Ti:Sapphire laser produces a series of sub-picosecond optical pulses at a central wavelength of 800 nm and a repetition rate of 80 MHz. The laser output is split into a pump beam and a probe beam by a polarizing beam splitter. The pump pulses are sinusoidally modulated by an electro-optic modulator (EOM) at frequencies up to 10 MHz, and then passed through a Bismuth Triborate (BiB_3O_6, or "BiBO") crystal that applies a second harmonic generation to the incident light,[85] therefore converting the pump pulses to 400 nm. The probe pulses are delayed up to 7 ns relative to the pump pulses with a mechanical delay stage—in our current approach to TDTR/FDTR measurements without metal transducer, this delay is the first step used to assess the time after pump excitation in which the majority of the excited carriers have relaxed, thereby ensuring the measured change in reflectivity is dominated by the thermoreflectivity component. To achieve these time delays, we use a doubling approach of the probe path on the delay stage as shown in Fig. 1, as opposed to the common approach of using multiple retroreflectors. A λ/2-wave plate is adjusted to ensure the probe beam is *p*-polarized and gets fully transmitted through a polarizing beam splitter.

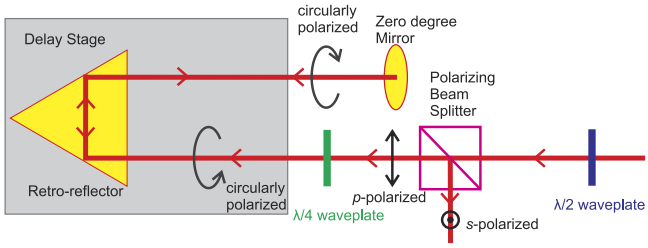

FIG. 1. A schematic showing the method of doubling the probe path over the delay stage in our TDTR/FDTR setup. A λ/2 wave plate sends the *p*-polarized light into a polarizing beam splitter. Then a λ/4 wave plate converts the linearly polarized light into circularly polarized light. The light is reflected by a retro-reflector and then reaches a zero-degree mirror, which reflects the light back along the same path. By adjusting the λ/4 wave plate, the reflected light can be converted into partially *s*-polarized, so that this component is reflected by the beam splitter.

A λ/4-wave plate is adjusted so that its fast axis is at 45° with probe polarization to convert the linearly polarized light into circularly polarized light. The probe is reflected by the retro-reflector to reach a zero-degree mirror, which reflects the light back along the same path, doubling the distance traveled and the resulting time delay. The circularly polarized probe is then converted to *s*-polarized light and is totally reflected by the polarizing beam splitter after passing through the λ/4-wave plate. In practice, we find that sending the probe beam back along its same incident path helps to minimize unintentional misalignment in the delay stage. A dichroic mirror is then used to reflect the 400 nm pump light and transmit the 800 nm probe light onto the sample. Both the pump and the probe are coaxially focused on the sample by an objective lens. The change in reflectivity of the probe off the sample surface, which is coaxially aligned with the pump, is monitored with a balanced amplified photodetector (Thorlabs PDB450A-AC), and the resulting converted voltage is directed to a lock-in-amplifier that is synced to the pump-modulation frequency. We monitor the in-phase (V_{in}) and out-of-phase (V_{out}) components of this lock-in signal.

III. DIRECT TDTR/FDTR PROBING PROCEDURE

A. Thermal and carrier effects

Photothermal reflectance signal generation in semiconductors can be understood in terms of the induced modulation of the refractive index. There are two mechanisms that contribute to the modulation of refractive index: the thermal effect due to the local temperature change and the plasma effect due to excited carrier density. Thus, the total photoreflectance signal change can be expressed as the sum of these two components[86]

$$\Delta R = \frac{\partial R}{\partial T}\Delta T + \frac{\partial R}{\partial N}\Delta N, \tag{1}$$

where $\partial R/\partial T$ is the temperature reflectance coefficient and $\partial R/\partial N$ is the free-carrier reflectance coefficient. These two coefficients of reflectance can be opposite in sign,[69,86] resulting in a partial net cancellation of the observed signal. In order to satisfy assumption (i) in nonmetals, an appropriate delay time must be determined at which to perform FDTR such that the carrier contribution to the reflectance signal is negligible compared to the thermal contribution.

Several prior works have studied the variations in reflectivity caused by the relative contributions from the thermal and plasma effects. Previous works by the Mandelis group[87,88] have discussed that the relative importance of the two mechanisms, which in the first approximation is determined by the $\omega\tau$ product, where $\omega = 2\pi f$ is the angular modulation frequency, and τ is the lifetime of the photoexcited free carriers. For $\omega\tau \ll 1$, the change in reflectivity is mainly due to the local temperature rise since the excited carriers have decayed. Therefore, at low frequencies, the photothermal reflectance signal has predominantly thermal origins. In our work, the measurements on the samples without a metal film transducer were carried out in the frequency range of 10 kHz–1 MHz, which is in the regime where

the thermal effects dominate the photothermal response and the plasma contribution to the response is negligible in our samples.

Furthermore, Guidotti and van Driel[89] have shown that the photoexcited carriers thermalize to the lattice temperature within a few picoseconds in Si; therefore, after relaxation of these photoexcited carriers in which a temperature can be defined, any excess energy contributed by non-radiatively recombined phonons is thermalized into the Bose-Einstein distribution during the time prescribed by our FDTR/TDTR measurements. Regardless, it is important to note that we conduct our measurements in the "low temperature perturbation" regime, so any deviation from equilibrium distributions is assumed small, as we validate with various pump and probe powers, described in more detail in Section III D.

Another consideration when determining the delay time is laser wavelength. Salnick and Opsal[90] demonstrated the role of the pump and probe wavelengths on the thermal and plasma wave behavior, concluding that with a 400 nm (3.1 eV) pump and 800 nm (1.55 eV) probe (the wavelengths we applied for our TDTR/FDTR measurements), thermal wave effects are the primary mechanism affecting the change in reflectivity. Therefore, our proposed approach ensures that our TDTR/FDTR measurements are always directly probing the thermal transport (and not carrier transport) in our systems since: (1) the modulation frequency that we employ during our measurements ensures $\omega\tau \ll 1$; (2) the pump and probe wavelengths we use ensure the thermal wave effects are dominated in our measured reflectivity; and (3) the pump-probe delay time that we select to conduct our measurements is a time that is greater than the carrier relaxation time.

While these aforementioned studies provide rough criteria for minimizing carrier effects on reflectance, the choice of time delay ultimately depends on material properties and pump/probe properties. Since the technique described here relies on pulsed-pulsed (pump-probe) FDTR, we make use of the fact that pump pulses arriving at the sample are separated temporally by 12.5 ns. Thus, it is sufficient to study the time domain solution to the coupled thermal and carrier responses described in Refs. 4 and 86. As such, we follow the approach outlined by Tanaka *et al.* (Eqs. (14)–(18) in Ref. 69). Figure 2 shows that for Si and GaAs, the carrier relaxation occurs on the order of 10–100 ps such that reflectivity is dominated by thermal response thereafter. The parameters used in the calculations are listed in Table I. Moreover, a previous report also shows that the relaxation time for silicon is on the order of 200 ps for similar experimental conditions as ours (including pump and probe wavelengths).[69] As such, in the following experiments, we performed the FDTR measurements at a time delay of 5 ns, sufficiently long enough to avoid any carrier effects on reflectivity.

Finally, previous report by Johnson *et al.*[81] shows that the carrier recombination time measured is on the order of 1.7-10 ns for Si depending on the period spacings of the gratings in their work. They assert that since the ambipolar carrier diffusion coefficient in Si is about an order of magnitude greater than the thermal diffusivity, the electronic and thermal relaxations are well separated in the time domain. In this context, they use a biexponential fit to their experimental

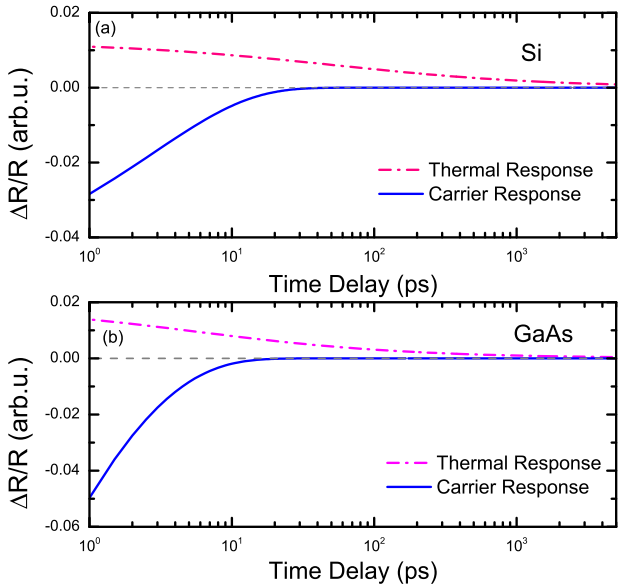

FIG. 2. Thermal and carrier contributions to the measured reflectance change during the pump-probe measurement. The calculations are based on Eqs. (14)–(18) in Ref. 69.

data and characterize the faster transient decay as due to carrier relaxation effects, which depends strongly on the carrier concentrations. The longer decay is related to thermal effects and most significantly the measured decay rates are shown to not depend on the different pump energies and initial carrier concentrations. Their findings along with other prior works suggest that carrier dynamics in semiconductors are not an intrinsic property of the material but highly depend on extrinsic variables such as laser fluence, photonic energy, and laser excitation pulse-width, as we discussed above. Therefore, a direct "apples-to-apples" comparison between the carrier relaxation rates in the work of Johnson *et al.*[81] and that reported in our work cannot be made; as we point out above, the calculated relaxation time in Si with the experimental parameters in our work is <1 ns. However, in line with the work of Johnson *et al.*, we find that with the judicious choice of pump and probe powers, the FDTR signals at longer time delays (5 ns) with varying powers are relatively constant (within experimental uncertainty, as described later

TABLE I. Parameters used in the calculations of Figure 2: γ_3 is the Auger recombination coefficient,[91,92] D_N is the ambipolar diffusion coefficient,[93] S is the surface recombination velocity,[67,94] E_g is the bandgap,[95] D_T is the thermal diffusivity,[95] $\tilde{n}$ is the complex refractive index,[70] n_1 is the real part of $\tilde{n}$,[96] N is the carrier density,[69] and T is temperature.

Parameter	Silicon	GaAs
γ_3 (cm^6/s)	7×10^{-30}	4×10^{-3}
D_N (cm^2/s)	20	10
S (cm/s)	2.4×10^5	5×10^5
E_g (eV)	1.1	1.43
D_T (cm^2/s)	0.85	0.28
$\tilde{n}$	$5.57+0.39i$	$4.46+2.08i$
$\partial n_1/\partial N$ (cm^3)	-4.4×10^{-22}	-4.4×10^{-22}
$\partial n_1/\partial T$ (K^{-1})	5.1×10^{-4}	2.0×10^{-4}

in Section III D—cf., Fig. 5), even though the signals at shorter time delays (~200 ps where carrier concentration effects are dominant) demonstrate statistically significant different signals at varying pump energies. Therefore, using the same procedure as Johnson *et al.*,[81] we support that at the time scales and laser powers studied in this work, the reflectivity change in the data presented in our manuscript is strictly in the thermally dominated regime and the carrier induced reflectivity change has negligible effect.

B. Thermal model with finite optical penetration

The thermal model traditionally used for analyzing TDTR or pulsed FDTR data is based on solving the classical heat diffusion equation while accounting for the pulse accumulation effect due to the high repetition rate of the laser.[5,6,72,73,97] As previously discussed, usually, with a metal transducer, the optical penetration depth of metals is very small (~10 nm) and the heat source can be considered as a surface heat source. As outlined in Section I, Yang *et al.*[78] have discussed the limitations of using a surface heat source in this traditionally assumed thermal diffusion model and utilized a convenient simplification when the probe's optical penetration depth is less than the heater penetration depth. In our case, we do not make this assumption regarding the relative pump and probe penetration depths in our implementation for data fitting, as some of the semiconductors of interest exhibit optical penetration depths that are comparable to the radius of our pump and probe beams (e.g., in silicon, the optical penetration depth at 800 nm is ~9.73 μm; note, the optical penetration depth is the inverse of the optical absorption coefficient).[70] Therefore, we implement a generalized thermal diffusion model applied in TDTR/FDTR analyses to include a z-dependent heat source and probe sampling depth. As a result, the heat diffusion equation in cylindrical coordinates is given by

$$\frac{\kappa_r}{r}\frac{\partial}{\partial r}\left(r\frac{\partial T(z,r,t)}{\partial r}\right)+\kappa_z\frac{\partial^2 T(z,r,t)}{\partial z^2}+\frac{1}{\varsigma}S(r,t)\exp\left(\frac{-z}{\varsigma}\right)=\rho c_p\frac{\partial T(z,r,t)}{\partial t}, \quad (2)$$

where κ_r and κ_z are the in-plane and cross-plane thermal conductivities, respectively, ρ is the mass density, c_p is the specific heat capacity (and the volumetric heat capacity is $C = \rho c_p$), and ς is the optical penetration depth of the pump beam; in the remainder of this work, we refer to ς as the heat penetration depth to distinguish it from the optical penetration depth of the probe beam.[98] We note that the heat penetration depth is the depth to which the laser energy is deposited into the sample and is not the thermal penetration depth, which is related to the depth in which the modulated thermal wave extinguishes into the sample (the thermal penetration depth, which is modulation frequency dependent, is given by $\delta_{thermal} = \sqrt{\kappa/\pi\rho c_p f}$, where f is the modulation frequency of the heat source). $S(r,t) = \frac{2}{\pi r_0^2}\exp\left(\frac{-2r^2}{r_0^2}\right)g_0(t)$ is the source term resulting from the heat flux across the top surface,[6] where r_0 is the $1/e^2$ Gaussian pump beam radius and $g_0(t)$ is a function of time that includes the power absorbed by the sample at the pump wavelength. Taking the Fourier transform and Hankel transform of Eq. (2), we obtain

$$-\kappa_r k^2 \boldsymbol{T}(z,k,\omega)+\kappa_z\frac{\partial^2 \boldsymbol{T}(z,k,\omega)}{\partial z^2}+\frac{1}{\varsigma}\boldsymbol{S}(k,\omega)\exp\left(\frac{-z}{\varsigma}\right)=\rho c_p i\omega \boldsymbol{T}(z,k,\omega), \quad (3)$$

where ω is the angular frequency, k is the Hankel transform variable, and $\boldsymbol{T}(z,k,\omega)$ and $\boldsymbol{S}(k,\omega)$ are the Fourier and Hankel transform of $T(z,r,t)$ and $S(r,t)$, respectively. By solving Eq. (3) with an adiabatic boundary condition at the top surface and a semi-infinite boundary condition at the bottom surface, we can obtain the temperature profile function $\boldsymbol{T}(z,k,\omega)$.

The reflectance change ΔR due to the heating events can be assumed to be linearly proportional to the surface temperature change: $\Delta R = \beta T(r,t)$, where β is the thermoreflectance coefficient, assuming this is the primary mechanism driving the reflectivity change. Stated differently, the change in surface temperature is monitored by the change of the reflectance of the probe beam, assuming the modulated reflectivity of the probe beam is driven by temperature. Then the reflected probe beam intensity, $p_r(r,t)$, can be expressed as weighting the incident probe beam intensity function through the temperature variation and integrating it over the film thickness[6,78,99]

$$p_r(r,t) = \int_0^\infty p_i(r,t)\exp\left(\frac{-z}{\delta}\right)\beta T(z,r,t)\,dz, \quad (4)$$

where δ is the optical penetration depth of the probe. $p_i(r,t) = \frac{2}{\pi r_1^2}\exp\left(\frac{-2r^2}{r_1^2}\right)g_1(t)$,[5] where r_1 is the $1/e^2$ Gaussian probe beam radius and $g_1(t)$ is a function of time that includes the power in the probe beam. Finally, the frequency response of $p_r(r,t)$, denoted as $p_r(r,\omega)$, can be obtained by performing a Fourier transform Eq. (4). The pulse accumulation effect of the model is evoked in identical fashion as that outlined in Refs. 6 and 78.

In Figure 3, we show a representative TDTR/FDTR measurement of an intrinsic silicon (100) wafer that was probed directly with our system (i.e., no metal transducer), and the resultant fits with both a surface heat source model and with z-dependent heat source model; for these analyses, we fit only the radial (in-plane) thermal conductivity of the silicon (κ_r), where all other inputs to the model are assumed constant (listed in the caption of Figure 3). We note that silicon is isotropic, so we expect $\kappa_r = \kappa_z$ in this system. For relatively high thermal conductivity materials, this approach of TDTR/FDTR without the use of metal transducer will consistently sample κ_r, as we discuss in detail in Section IV B. If the sample is isotropic, such as those studied in this work, then our measurement provides a unique metrology to measure $\kappa = \kappa_r = \kappa_z$ and also provides a method to measure the thermal conductivity of materials without the potential for anisotropic failure of Fourier diffusion around the metal transducer/sample interface.[100] In the situation where the material is anisotropic, our described implementation of TDTR/FDTR is most sensitive to in-plane transport for

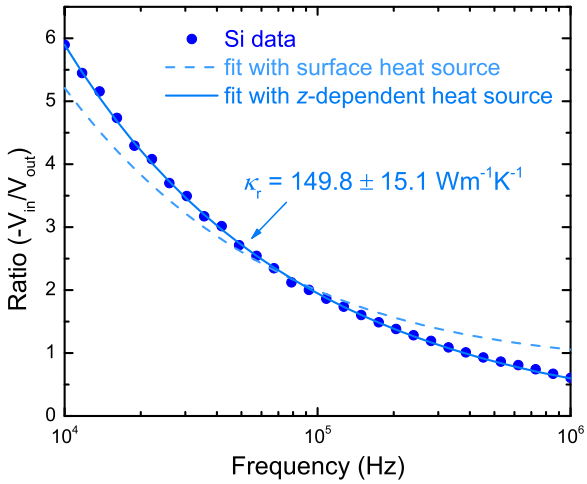

FIG. 3. Model fits to TDTR/FDTR measurements of an intrinsic silicon (100) wafer without a metal transducer (henceforth referred to as "bare") at a TDTR delay time of 5 ns. Fitting with z-dependent heat source (solid line) results in an in-plane thermal conductivity best fit value of κ_r = 149.8 ± 15.1 W m^{-1} K^{-1}, while fitting with surface heat source (dashed line) results in poor goodness of fit for silicon. The parameters used in fitting our model to the data are as follows: volumetric heat capacity of Si $C = 1.63 \times 10^6$ J m^{-3} K^{-1} (Ref. 95), pump beam radius = 11.3 μm, probe beam radius = 9.5 μm, optical penetration depth δ and heat penetration depth ς are calculated with $\delta = \lambda/4\pi n_2$, where λ is 800 nm and 400 nm for probe beam and pump beam, respectively, n_2 is the extinction coefficient. From this, δ = 9.73 μm and ς = 97.90 nm.[102] The uncertainty of the thermal conductivity value comes from ±5% variations of the pump and probe beam radii used in the fitting model.

relatively high κ_z systems, as discussed in more detail in our sensitivity analysis and limitations outlined in Section IV.

The data in Figure 3 were collected at a TDTR delay time of 5 ns, and the selection of this time is discussed in detail in Sec. III C. The z-dependent heat source model provides a good fit to the experimental data and results in a best fit thermal conductivity of Si of κ_r = 149.8 ± 15.1 W m^{-1} K^{-1} (uncertainty comes from ±5% variations of pump and probe beam radii used in fitting the model to the data), consistent with literature.[101] Performing a fit with the model assuming a surface heat source results in a poor goodness of fit.

The results in this section demonstrate the ability to perform FDTR measurements at a specified TDTR delay time (i.e., a hybrid TDTR/FDTR approach) without the use of a metal film transducer (henceforth, these samples are referred to as "bare" to indicate the lack of metal coating). The intricacies and procedures to this approach are outlined in Secs. III C and III D.

C. Fitting at different delay times

Our analysis relies on the fact that the measured change in modulated reflectance is dominated by the thermoreflectance component, as discussed in Section III A. Therefore, we select delay times in which to perform our FDTR measurements that ensure that the non-thermoreflectance contributions to the modulated reflectivity signal are minimized. This is the same principle that was used in previous TDTR[79,80] and transient grating procedures.[81,83] However, unlike in these works, we posit that we can utilize the frequency domain response (i.e., FDTR) at these judiciously chosen time delays in which the non-thermoreflectivity components to modulated reflectance have been minimized, thereby generalizing our approach to any non-metal without the use of surface modification in a standardized TDTR geometry. Therefore, by performing FDTR measurements at much longer delay times and accounting for the out-of-phase response of the FDTR signal, which, given low enough modulation frequencies, will be dominated by the heating of the pump, we can relate the FDTR signal to the thermal diffusion equation outlined in Sec. III B. This forms the basis of our hybrid TDTR/FDTR approach. Hence, in practice, our approach is based on performing TDTR measurements at different frequencies.

We show examples of this fitting approach for GaAs (100) wafers. Figure 4(a) shows the normalized in-phase component of the lock-in amplifier signal (V_{in}) as a function of pump-probe delay time collected at a pump frequency of 10 MHz. The changes in this measured signal near time t = 0 ps correspond to the hot carrier dynamics from the absorption of the pump beam. After a few hundred picoseconds, this component of the signal relaxes, which corresponds to the extinction of the excited carrier portion of the reflectivity.[103] While the thermoreflectivity component is also relaxing during this time, the carrier portion has been shown to relax more rapidly than the thermal portion. At ~1 ns, the real component of the signal is nearly fully relaxed, and the lock-in amplifier signals will be dominated by the thermoreflectivity component of the modulated reflectivity measurements. Therefore, FDTR measurements should be performed at a delay time after this time regime when the in-phase component is minimized. As typical with TDTR and FDTR analyses, after this time, we then analyze the ratio of the in-phase to out-of-phase signal ($-V_{in}/V_{out}$), since the out-of-phase component is still appreciable due to the thermomodulation component of the reflectivity, which is driven by the thermal properties of the samples. Due to this, we perform FDTR measurements at relatively low modulation frequencies to induce a larger out-of-phase signal; we discuss the implications of this selection in more detail in Section IV.

Figures 4(b)–4(f) show the FDTR measurements of the same GaAs wafer at delay times of −10 ps, 200 ps, 1 ns, 3 ns, and 5 ns, respectively. The corresponding fitted thermal conductivities using the model discussed in Section III A are listed in the plots; we note, again, that these thermal conductivities are κ_r, as we are insensitive to κ_z for GaAs over the frequency domain utilized in this work, as discussed in more detail in Section IV B. At all sampled delay times, except for t = 200 ps, the model fits the data well and results in best fits to the thermal conductivity that are consistent among each other and with previous reports in the literature. At 200 ps, the measured GaAs signal is not entirely dominated by the thermoreflectivity component, rendering our thermal diffusion model invalid to analyze the data. The monitoring of the in-phase component of the signal as a function of time to determine when to fit $-V_{in}/V_{out}$ in the FDTR analysis is key to this approach. In the following discussions, we fit all FDTR data at a delay time t = 5 ns.

To further validate our approach of analyzing the FDTR signal at time-delays after the carrier reflectivity has relaxed,

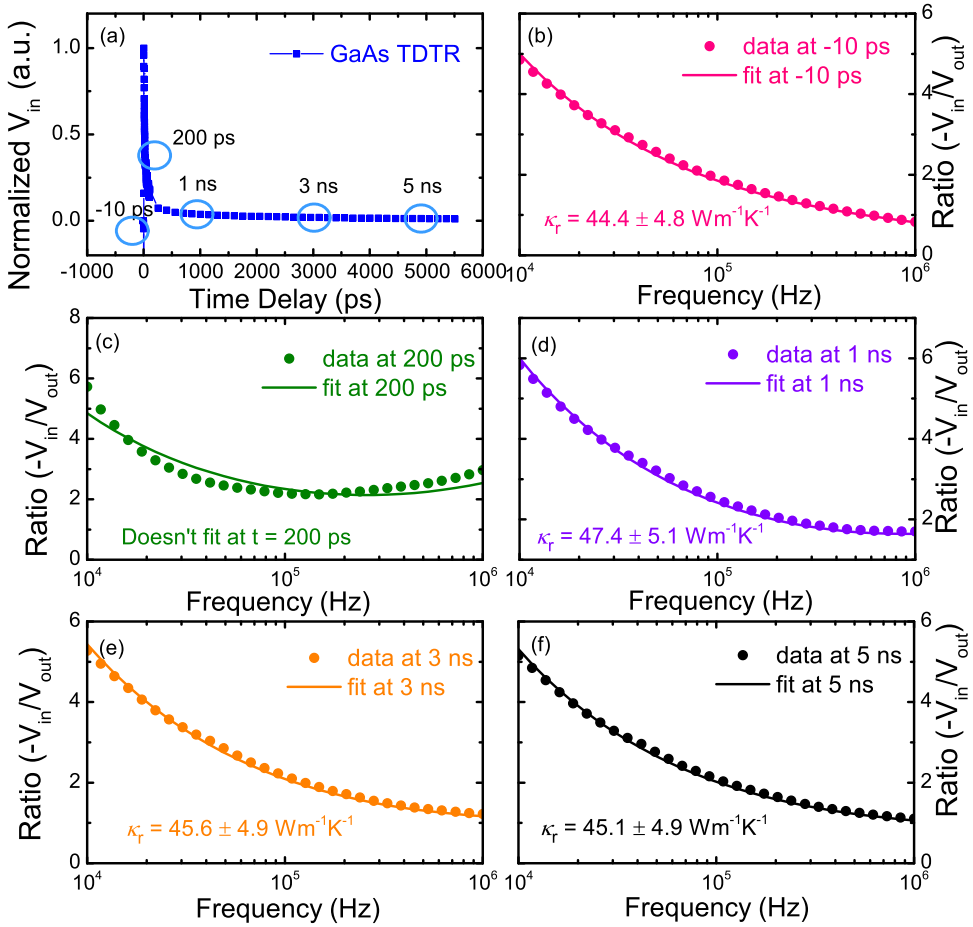

FIG. 4. (a) In-phase TDTR signal on a "bare" (non-metal coated) GaAs (100) wafer at a modulation frequency of 10 MHz. Five delay times are chosen to perform FDTR measurements as shown in (b) $t = -10$ ps ($t = 12.490$ ns), (c) $t = 200$ ps, (d) $t = 1$ ns, (e) $t = 3$ ns, and (f) $t = 5$ ns. The thermal conductivities fitted at different delay times are shown in each figure. The data at $t = 200$ ps result in a poor fit due to the measured modulated reflectivity exhibiting components that are not dominated only by the thermoreflectivity of the GaAs. The parameters used in the fitting model: volumetric heat capacity of GaAs $C = 1.76 \times 10^6$ J m^{-3} K^{-1} (Ref. 104) pump beam radius = 11.3 μm, probe beam radius = 9.5 μm.

we performed the same analysis on lightly doped p- and n-type silicon wafers (resistivities around 1-10 Ω-cm). For these doped wafers, at a short time regime (a few picoseconds), the TDTR signals are different than those of intrinsic semiconductors due to different carrier excitation responses. However, fitting these doped Si data at 5 ns results in the same best-fit thermal conductivities (within uncertainty) as the intrinsic sample shown in Figure 3, further validating the strength of our approach.

D. Ensuring perturbative temperature rise and power independence

We perform the FDTR measurements over the frequency regime shown in Figures 3 and 4 to ensure a large enough out-of-phase signal to confidently fit $-V_{in}/V_{out}$, even though the time-delay is large enough such that V_{in} is relatively small compared to that at earlier delay times. However, with decreasing modulation frequency, the steady-state temperature rise created by the average laser power as well as the temperature oscillations created by the modulation of the pump beam can lead to a non-negligible heating event that can lead to sources of error in the FDTR analysis. In our FDTR measurements, the probe power is 2 mW, and the pump power is carefully chosen to achieve an acceptable signal while avoiding too large of a temperature rise (<8 K for the GaAs data). For the samples interrogated in this work, the temperature rise from the average steady state laser power is relatively negligible due to the high thermal effusivity of the wafers; however, the modulated temperature rise must be monitored.

Following the work by Cahill *et al.*[5,105] the temperature rise induced by the modulation of the pump beam of a thermally thick layer can be estimated as $\Delta T = A/\pi r_0^2\sqrt{2\pi f \kappa C}$ in the high frequency limit ($f \gg D/2\pi r_0^2$) and $\Delta T = A/2\sqrt{\pi} r_0 \kappa$ in the low frequency limit ($f \ll D/2\pi r_0^2$), where A is the amplitude of the absorbed power from the pump beam,[62] r_0 is the pump beam radius, f is the modulation frequency, κ is the thermal conductivity, C is the volumetric heat capacity, and D is the thermal diffusivity. Therefore, as the frequency is lowered, the temperature rise induced by the modulated pump train becomes more pronounced. In Fig. 5(a), we show FDTR measurements on GaAs with different pump powers in the low frequency range from 1.0 to 100 kHz. The measured FDTR signals clearly change with different pump powers. With low powers (4 mW, 12 mW, and 30 mW), the signals

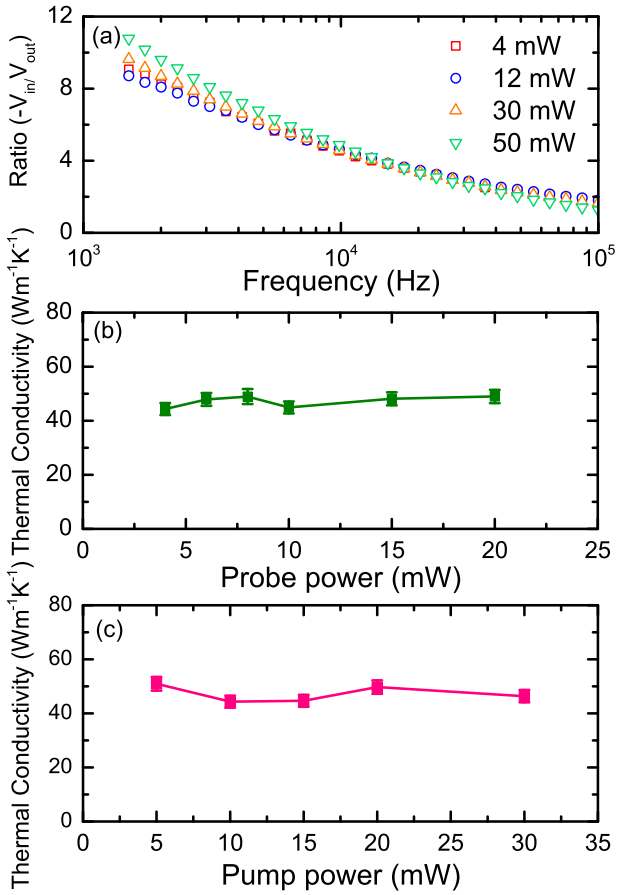

FIG. 5. (a) Experimental FDTR data of a bare GaAs (100) wafer measured with different pump powers. (b) Fitted thermal conductivities of GaAs wafer by varying probe power with pump power of 10 mW. (c) Fitted thermal conductivities of GaAs wafer by varying pump power with probe power of 4 mW.

diverge at low frequencies yet converge at high frequencies (>7 kHz), consistent with the discussion of non-perturbative heating as frequency is lowered. So we performed FDTR measurements with frequency range starting from 10 kHz. For the data collected at the highest power shown in this figure (50 mW), the shape of the signal changes substantially and cannot be fit with our thermal model, indicating that the average temperature oscillations are too high to assume a relatively constant temperature over the entire frequency range, in addition to other potential factors that are not accounted for in our linear perturbation thermal analysis, such as increased carrier lifetimes that would lead to the $\omega\tau$ product not $\ll 1$. From this, we assert that when collecting FDTR data, several powers should be used to ensure that the fitted data lie in a regime of a relatively small and linear temperature perturbation. This can also be checked by comparing the normalized in-phase response as a function of time. The importance of pump power in measuring the FDTR in the linear perturbation thermoreflectance-dominated response regime is also exemplified in our previous discussion regarding the carrier dynamics (Section III A). Figures 5(b) and 5(c) show the measured thermal conductivities of GaAs at various pump and probe powers. As shown in these figures, within uncertainties, the measured thermal conductivities do not show a dependence on the pump and probe powers. This check should be performed to ensure that the data are collected in a regime where the thermal signal dominates the measured reflectivity (negligible carrier component); note, this procedure is consistent with the similar check used in the transient grating experiments described by Johnson *et al.*[81]

IV. DATA ANALYSIS AND SENSITIVITIES

A. FDTR data and calibration with and without a metal transducer

We demonstrate the applicability of this approach by performing this TDTR/FDTR procedure on both bare intrinsic Si (100), GaAs (100) (from MTI corporation and University-Wafer), and InSb (100) wafers along with a portion of the same wafers coated with ~80 nm of Al (a more traditional FDTR approach), as shown in Fig. 6. The only difference between these two measurements shown in each plot is the aluminum metal transducer layer. The measurements were performed over a frequency range of 10 kHz–1 MHz at a delay time of 5 ns. Fitting was performed using a nonlinear least-squares minimization routine. The spot radii used in the fitting were 11.3 μm for the pump beam and 9.5 μm for the probe beam, which were calibrated with FDTR measurements, as discussed in more detail in Section IV B. We assumed literature values for the volumetric heat capacity C for Si ($C = 1.63 \times 10^6$ J m^{-3} K^{-1}),[95] GaAs ($C = 1.76 \times 10^6$ J m^{-3} K^{-1}),[104] and InSb ($C = 1.15 \times 10^6$ J m^{-3} K^{-1}).[106] The optical penetration depths for each sample δ were calculated as $\delta = \lambda/4\pi n_2$, where λ is 400 nm and 800 nm for pump beam and probe beam, respectively, n_2 is the extinction coefficient. We assume that the optical penetration depth of the pump is equivalent to the heat penetration depth, ς.[78]

We find that only Si needs to be fitted with a z-dependent heat source model due to the large optical penetration depth of the probe compared to the heat penetration depth ($\delta_{Si} = 9.73$ μm, $\varsigma_{Si} = 97.90$ nm).[102] For GaAs and InSb, the optical penetration depths are smaller and the heat penetration depths are near surface and metal like at 400 nm ($\delta_{GaAs} = 0.74$ μm, $\varsigma_{GaAs} = 14.84$ nm, $\delta_{InSb} = 91.26$ nm, $\varsigma_{InSb} = 15.79$ nm),[102] and in this limit, a surface heat source can be assumed in the solution to the diffusion equation (similar to a traditional FDTR/TDTR analysis with a metal film transducer). As an example, take GaAs; the fitted thermal conductivity of GaAs (100) wafer from MTI corporation is $\kappa_r = 45.1 \pm 4.9$ W m^{-1} K^{-1} when using surface heat source model, and $\kappa_r = 45.0 \pm 4.7$ W m^{-1} K^{-1} when using z-dependent heat source model. As a result, the surface heat source solution can be assumed for fitting the data of GaAs and InSb. The free parameter in all measurements on the bare samples is only the thermal conductivity of the sample. For samples with the Al transducer layer, the Al/semiconductor interface conductances used as input parameters in the FDTR fits are measured with TDTR at 10 MHz.

Figure 6 shows experimental data and the best-fit curves. The fitted thermal conductivities for each sample are shown in each figure. As shown in figure, the thermal conductivities measured with the Al layer and direct FDTR probing

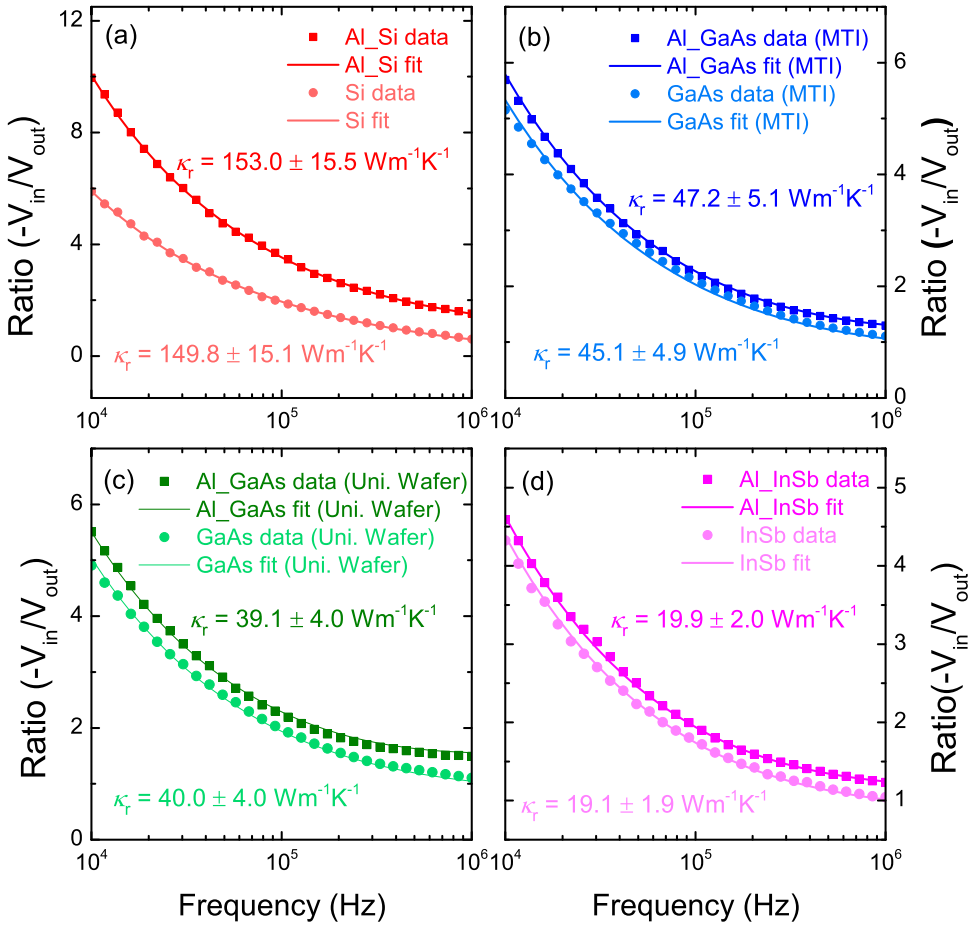

FIG. 6. Data points (symbols) and best fit curves (solid lines) for the FDTR measurements on (a) intrinsic Si (100), (b) GaAs (100) (MTI), (c) GaAs (100) (University Wafer), and (d) InSb (100). The FDTR measurements of the same wafers with 80 nm Al layers are also shown in figure. The fitted thermal conductivities are shown for each case. The FDTR measurements are performed in a frequency range of 10 kHz–1 MHz and at a delay time of 5 ns. For samples with Al layer, the Al/semiconductor interface conductance h used in FDTR fits is measured with TDTR method at 10 MHz: $h_{\mathrm{Al/Si}} = 2.0\times10^{8}$ W m^{-2} K^{-1}, $h_{\mathrm{Al/GaAs}} = 8.5\times10^{7}$ W m^{-2} K^{-1}, and $h_{\mathrm{Al/InSb}} = 5.1\times10^{7}$ W m^{-2} K^{-1}.

agree within experimental uncertainty, indicating the potential for this procedure to measure the thermal conductivity of materials without a metal transducer.

B. Sensitivity analysis and sources of error

To quantify the sensitivity of the various experimental parameters in this direct probing TDTR/FDTR method, we use the approach by Costescu *et al.*,[107] where the sensitivity of the ratio to a parameter x is defined by $S_x = \partial(-V_{in}/V_{out})/\partial \ln(x)$. We calculated the sensitivities for the in-plane thermal conductivity, cross-plane thermal conductivity, and spot size. For Si, since we applied the z-dependent heat source model, we also show the sensitivity analysis of optical penetration depth and heat penetration depth. The results are shown in Fig. 7 for (a) InSb, (b) GaAs, and (c) Si. The sensitivity analysis is performed over a frequency range of 1 kHz–10 MHz with a delay time of 5 ns. Clearly, direct FDTR probing is sensitive to the in-plane thermal conductivity while insensitive to the cross-plane thermal conductivity, since there is no significant temperature gradient in the cross-plane direction compared to the in-plane direction at these heat penetration depths and modulation frequencies. As a result, this technique can be used to measure in-plane thermal conductivities. Although for the isotropic samples interrogated in this work, the in- and cross-plane thermal conductivities can be assumed identical, for anisotropic samples or layered structures, our approach could present a method to measure the in-plane thermal conductivity. We do not pursue this approach in our current work but offer this as a potential future direction.

We also note that the samples examined in this work have relatively high thermal conductivities when compared to glassy/disordered or nanostructured samples designed to minimize phonon thermal transport. For relatively low thermal conductivity samples, the heating induced by the pump power could lead to non-negligible heating, rendering our assumption of a relatively constant temperature invalid. While in principle this heating could be accounted for via more sophisticated analyses, it is beyond the scope of this present work. However, as the thermal conductivity of the sample is reduced, the temperature gradients in the cross-plane direction become more pronounced, and if the penetration depths are relatively shallow, this approach can be applied to measure the cross-plane thermal conductivity. Again, we leave this as a potential future direction of this TDTR/FDTR procedure.

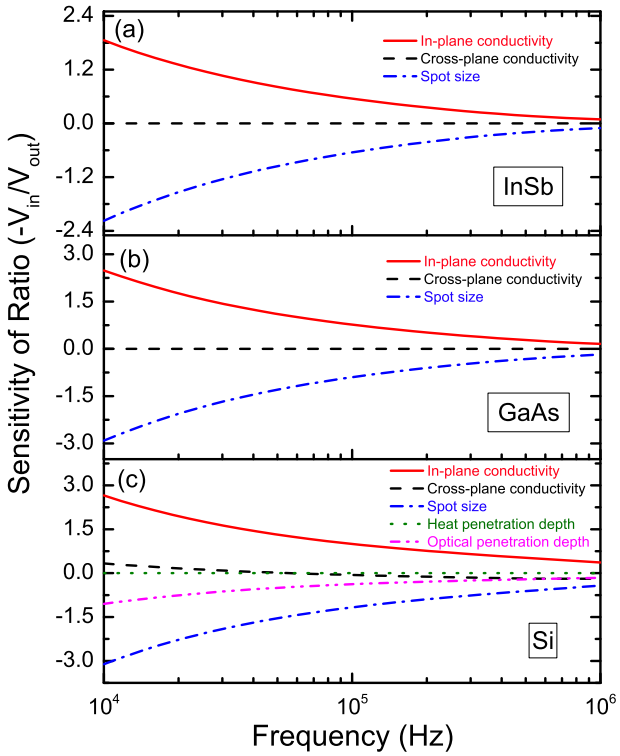

FIG. 7. FDTR measurement sensitivity of the ratio $(-V_{in}/V_{out})$ to the in-plane thermal conductivities, cross-plane thermal conductivities, and the laser spot size for (a) InSb, (b) GaAs, and (c) Si. Since the fitting model used for Si includes the z-dependent heat source, the sensitivities to the heat penetration depth and optical penetration depth are included.

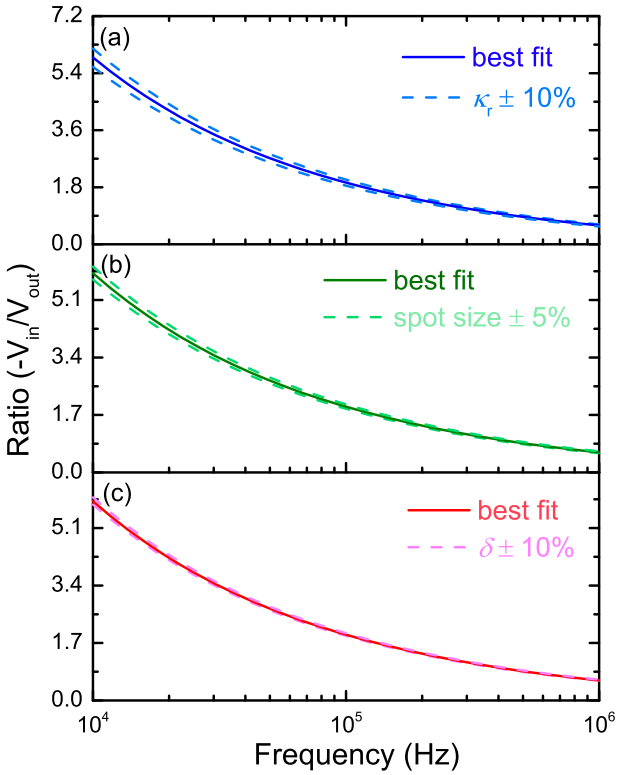

FIG. 8. Best-fit curve for Si and curves varied by (a) thermal conductivity $\kappa \pm 10\%$, (b) spot size $\pm 5\%$, and (c) optical penetration depth $\delta \pm 10\%$. 5% variations in spot size cause nearly 10% off in thermal conductivities. All plots are at a time delay of 5 ns.

As apparent from Fig. 7, direct FDTR probing is very sensitive to the spot size and optical penetration depth. In fact, for the Si, the penetration depths offer very similar sensitivities (opposite and similar magnitudes) to the thermal conductivity. In the fitting of our model to the data, we assumed literature values for the penetration depths, as fitting of this quantity can substantially increase the measurement uncertainty in determining the thermal conductivity. As we do not treat the penetration depths as free parameters, the main source of error in our technique is in the spot size.

In Fig. 8, we plot the best-fit curves for Si (fit curve shown in Fig. 6(a)), and also the curves by varying the thermal conductivity $\kappa_r \pm 10\%$ (Fig. 8(a)), pump and probe beam spot sizes ±5% (Fig. 8(b)), and optical penetration depth $\delta \pm 10\%$ (Fig. 8(c)). We can see 10% variation in δ negligibly affects the best fit thermal conductivities; however, the fitting curves of 5% variations in spot size are almost the same as those of 10% variations in thermal conductivity. As a result, 5% variation in spot size will cause around 10% error in the thermal conductivity measurements. To obtain accurate thermal conductivity values with direct FDTR probing, precise spot sizes are crucial.

We calibrated the spot sizes by performing FDTR measurements at a time delay of 5 ns on a SiO_2 substrate coated with 80 nm Al layer and fit the effective spot size with the data. FDTR measurements performed at this time delay are most sensitive to the effective pump and probe spot sizes assuming the metal film thickness is well known (which we measure with profilometry and picosecond acoustics using TDTR at the same measurement location). In Fig. 9(a), we show the sensitivity of the solution to the spot size, and for reference, substrate thermal conductivity at this time delay. Over this frequency range (200 kHz–10 MHz), the sensitivity of an FDTR measurement to the spot size dominates that of the thermal conductivity. As a result, we fit the effective spot size $\sqrt{r_0^2 + r_1^2}$ from the FDTR measurements in this frequency range as shown in Fig. 9(b), where r_0 and r_1 are the pump and probe radii, respectively. The fitted radii result in 13.6 μm for the pump beam spot and 5.5 μm for the probe beam spot. For comparison, the measured pump and probe radii with the knife-edge technique are 14.0 ($\pm$ 0.5) μm and 5.5 ($\pm$ 0.5) μm, respectively. The difficulty in interpreting these measurements originates from the fact that there is high uncertainty in precisely knowing the position of the exact sample plane at focus (during the TDTR/FDTR measurements) and that in the knife-edge. In this regard, the highest accuracy in precisely determining the spot size at the sample focus in our TDTR/FDTR measurements is with the method by using FDTR measurements at relatively low frequencies where the thermal model is highly sensitive to the effective spot size. Therefore, we assert that this method of using FDTR at long time delays when the measurement sensitivity to the spot size is relatively large provides a unique method to determine the spot sizes during thermoreflectance techniques via a self-consistent and *in situ* approach.

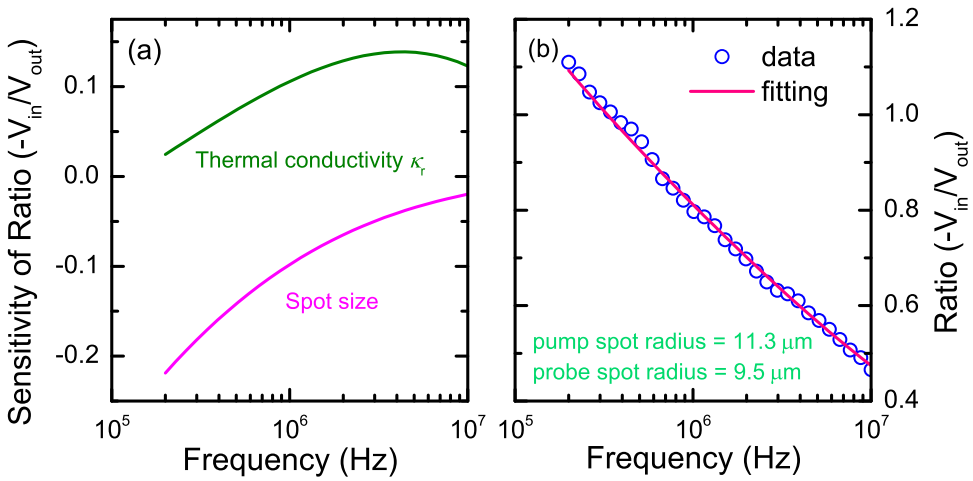

FIG. 9. (a) FDTR measurement sensitivity of the ratio ($-V_{in}/V_{out}$) to the thermal conductivities and the laser spot size of 80 nm Al/SiO_2 at a time delay of 5 ns. (b) FDTR fitting of beam spot sizes for 80 nm Al/SiO_2. All plots are at a time delay of 5 ns.

V. SUMMARY

The major results of our work are summarized in Fig. 10, which shows the thermal conductivities measured on bare wafers and on wafers with Al coatings by FDTR. The error bars in this figure comes from 5% variations of pump and probe beam sizes. In addition to our approach of probing the semiconductors directly without the use of a metal transducer agreeing with a more traditional FDTR approach with the metal film, our values also agree well with literature.[95,101,108,109] We note that the thermal conductivities of the GaAs purchased from two different vendors vary in magnitude, and this difference is captured with our procedure for FDTR without a transducer (and confirmed with a transducer). This difference in thermal conductivity of wafers from different manufacturers is not surprising, as the thermal conductivity of crystals is strongly influenced by defects that could be present in different companies' fabrication procedures.

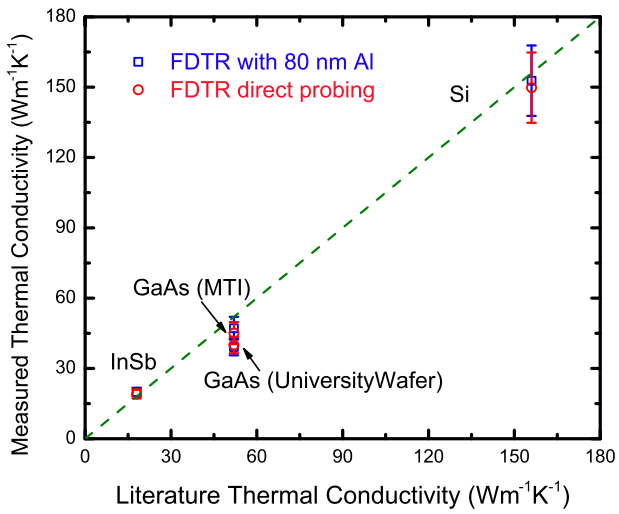

FIG. 10. Thermal conductivities of intrinsic Si (100), GaAs (100) (MTI and UniversityWafer), and InSb (100) measured on bard wafers and on the same wafers coated with 80 nm Al layers. The dashed green line is the reference line for literature values. The error bars come from 5% variations of pump and probe radii used in the fittings.

This work outlined a method to directly measure the thermal conductivities of bulk semiconductors without using a metal transducer layer using a standard TDTR/FDTR experiment. A major key in this approach was the use of a thermal model with z-dependent heat source when the optical penetration depth is comparable to the beam sizes, and measuring the FDTR response at a long delay time to minimize non-thermoreflectivity contributions to the modulated reflectance signals (such as free carrier excitations). We also discussed the frequency range and the pump power used in this method in order to avoid significant temperature rises due to pulse accumulation and modulated heating, while also checking to ensure the measured change in reflectivity is dominated by the thermal component with negligible influence from the carrier component. Using this approach, we demonstrated the ability to measure the thermal conductivity on three semiconductors, intrinsic Si (100), GaAs (100), and InSb (100), the results of which were validated with FDTR measurements on the same wafers with 80 nm Al transducers. Our sensitivity analyses show that the beam spot sizes are the main source of uncertainty when implementing this method; as a result, we also present a procedure to measure the effective spot sizes by fitting the FDTR data of an 80 nm Al/SiO_2 sample at a time delay in which the spot size sensitivity dominates an FDTR measurement over the substrate thermal properties. In this way, we can obtain accurate spot sizes via a self-consistent, *in situ* approach during our FDTR measurement.

The thermal conductivities that we measure on these samples in this work are technically the radial thermal conductivities; however, due to the cubic symmetry of the Si, GaAs, and InSb, we expect $\kappa_r = \kappa_z$. This, however, is not the case for samples with anisotropic crystal structures or layered nanostructures. While we do not pursue measurement of the in-plane thermal conductivity separately from the cross-plane for these aforementioned anisotropic samples, this is a potential direction for future works. Similarly, it is beyond the scope of this work to apply this measurement procedure to lower thermal conductivity samples due to the advent of large

temperature excursions and therefore a more complicated thermal model accounting for temperature dependent thermal properties. However, we note that as the thermal conductivity of the sample is reduced, the temperature gradients in the cross-plane direction become more pronounced, and if the penetration depths are relatively shallow, this approach can be applied to measure the cross-plane thermal conductivity. Again, we leave this as a potential future direction of this TDTR/FDTR procedure.

The experimental analysis presented in this work requires that the time scales associated with the plasma/excited carrier density effects on ΔR can be separated from the thermal effects on ΔR. As discussed in this work, the time scale of the plasma contribution depends significantly on the wavelength and modulation frequency used during a TDTR/FDTR experiment. For example, the fact that the photoexcited carriers in Si thermalize to the lattice temperature well before the time-delay chosen for our FDTR measurements allows for the correct interpretation and implementation of the thermal model used to analyze the data. However, it is important to note that for a material with unknown time scales of plasma contributions to the change in reflectivity (for the experimental parameters used), the uninformed implementation of this technique could result in erroneous measurements of thermal properties of the material. Therefore, for the correct implementation of the technique presented in this work, it is essential to characterize the effect of the plasma/excited carrier density effects on ΔR to ensure that the decay of the in-phase signal of the TDTR experiment can be an indicator of a pertinent time scale in which to conduct the FDTR thermal measurement; typically, this means conducting the TDTR/FDTR experiments at low modulation frequencies and at photon energies much greater than the bandgap. The extent to which the photon energies should be greater than the bandgap is material dependent.

ACKNOWLEDGMENTS

We appreciate support from the Air Force Office of Scientific Research (Grant No. FA9550-15-1-0079) and the Office of Naval Research (Grant No. N00014-15-12769).

[1]R. Rosei and D. W. Lynch, "Thermomodulation spectra of Al, Au, and Cu," Phys. Rev. B **5**, 3883–3894 (1972).
[2]G. L. Eesley, "Observation of nonequilibrium electron heating in copper," Phys. Rev. Lett. **51**, 2140–2143 (1983).
[3]C. A. Paddock and G. L. Eesley, "Transient thermoreflectance from thin metal films," J. Appl. Phys. **60**, 285–290 (1986).
[4]J. Opsal, A. Rosencwaig, and D. L. Willenborg, "Thermal-wave detection and thin-film thickness measurements with laser beam deflection," Appl. Opt. **22**, 3169–3176 (1983).
[5]D. G. Cahill, "Analysis of heat flow in layered structures for time-domain thermoreflectance," Rev. Sci. Instrum. **75**, 5119–5122 (2004).
[6]A. J. Schmidt, R. Cheaito, and M. Chiesa, "A frequency-domain thermoreflectance method for the characterization of thermal properties," Rev. Sci. Instrum. **80**, 094901 (2009).
[7]A. J. Schmidt, "Pump-probe thermoreflectance," Annu. Rev. Heat Transfer **16**, 159–181 (2013).
[8]D. G. Cahill, P. V. Braun, G. Chen, D. R. Clarke, S. Fan, K. E. Goodson, P. Keblinski, W. P. King, G. D. Mahan, A. Majumdar, H. J. Maris, S. R. Phillpot, E. Pop, and L. Shi, "Nanoscale thermal transport. II. 2003–2012," Appl. Phys. Rev. **1**, 011305 (2014).
[9]D. G. Cahill, W. K. Ford, K. E. Goodson, G. D. Mahan, A. Majumdar, H. J. Maris, R. Merlin, and S. R. Phillpot, "Nanoscale thermal transport," J. Appl. Phys. **93**, 793–818 (2003).
[10]R. Cheaito, J. T. Gaskins, M. E. Caplan, B. F. Donovan, B. M. Foley, A. Giri, J. C. Duda, C. J. Szwejkowski, C. Constantin, H. J. Brown-Shaklee, J. F. Ihlefeld, and P. E. Hopkins, "Thermal boundary conductance accumulation and interfacial phonon transmission: Measurements and theory," Phys. Rev. B **91**, 035432 (2015).
[11]R. B. Wilson and D. G. Cahill, "Limits to Fourier theory in high thermal conductivity single crystals," Appl. Phys. Lett. **107**, 203112 (2015).
[12]J. C. Duda, P. E. Hopkins, Y. Shen, and M. C. Gupta, "Thermal transport in organic semiconducting polymers," Appl. Phys. Lett. **102**, 251912 (2013).
[13]J. C. Duda, P. E. Hopkins, Y. Shen, and M. C. Gupta, "Exceptionally low thermal conductivities of films of the fullerene derivative PCBM," Phys. Rev. Lett. **110**, 015902 (2013).
[14]R. M. Costescu, D. G. Cahill, F. H. Fabreguette, Z. A. Sechrist, and S. M. George, "Ultra-low thermal conductivity in W/Al_2O_3 nanolaminates," Science **303**, 989–990 (2004).
[15]C. Chiritescu, D. G. Cahill, N. Nguyen, D. Johnson, A. Bodapati, P. Keblinski, and P. Zschack, "Ultralow thermal conductivity in disordered, layered WSe_2 crystals," Science **315**, 351–353 (2007).
[16]M. D. Losego, I. P. Blitz, R. A. Vaia, D. G. Cahill, and P. V. Braun, "Ultralow thermal conductivity in organoclay nanolaminates synthesized via simple self-assembly," Nano Lett. **13**, 2215–2219 (2013).
[17]X. Wang, C. D. Liman, N. D. Treat, M. L. Chabinyc, and D. G. Cahill, "Ultralow thermal conductivity of fullerene derivatives," Phys. Rev. B **88**, 075310 (2013).
[18]A. Giri, J.-P. Niemelä, C. J. Szwejkowski, M. Karppinen, and P. E. Hopkins, "Reduction in thermal conductivity and tunable heat capacity of inorganic/organic hybrid superlattices," Phys. Rev. B **93**, 024201 (2016).
[19]J. Liu, J. Zhu, M. Tian, X. Gu, A. Schmidt, and R. Yang, "Simultaneous measurement of thermal conductivity and heat capacity of bulk and thin film materials using frequency-dependent transient thermoreflectance method," Rev. Sci. Instrum. **84**, 034902 (2013).
[20]M. N. Luckyanova, J. Garg, K. Esfarjani, A. Jandl, M. T. Bulsara, A. J. Schmidt, A. J. Minnich, S. Chen, M. S. Dresselhaus, Z. Ren, E. A. Fitzgerald, and G. Chen, "Coherent phonon heat conduction in superlattices," Science **338**, 936–939 (2012).
[21]M. N. Luckyanova, J. A. Johnson, A. A. Maznev, J. Garg, A. Jandl, M. T. Bulsara, E. A. Fitzgerald, K. A. Nelson, and G. Chen, "Anisotropy of the thermal conductivity in GaAs/AlAs superlattices," Nano Lett. **13**, 3973–3977 (2013).
[22]J. Ravichandran, A. K. Yadav, R. Cheaito, P. B. Rossen, A. Soukiassian, S. J. Suresha, J. C. Duda, B. M. Foley, C.-H. Lee, Y. Zhu, A. W. Lichtenberger, J. E. Moore, D. A. Muller, D. G. Schlom, P. E. Hopkins, A. Majumdar, R. Ramesh, and M. A. Zurbuchen, "Crossover from incoherent to coherent phonon scattering in epitaxial oxide superlattices," Nat. Mater. **13**, 168–172 (2014).
[23]R. Cheaito, C. S. Gorham, A. Misra, K. Hattar, and P. E. Hopkins, "Thermal conductivity measurements via time-domain thermoreflectance for the characterization of radiation induced damage," J. Mater. Res. **30**, 1403–1412 (2015).
[24]R. Cheaito, K. Hattar, J. T. Gaskins, A. K. Yadav, J. C. Duda, T. E. Beechem, J. F. Ihlefeld, E. S. Piekos, J. K. Baldwin, A. Misra, and P. E. Hopkins, "Thermal flux limited electron Kapitza conductance in copper-niobium multilayers," Appl. Phys. Lett. **106**, 093114 (2015).
[25]P. Dongmo, Y. Zhong, P. Attia, C. Bomberger, R. Cheaito, J. F. Ihlefeld, P. E. Hopkins, and J. Zide, "Enhanced room temperature electronic and thermoelectric properties of the dilute bismuthide InGaBiAs," J. Appl. Phys. **112**, 093710 (2012).
[26]P. Chen, N. A. Katcho, J. P. Feser, W. Li, M. Glaser, O. G. Schmidt, D. G. Cahill, N. Mingo, and A. Rastelli, "Role of surface-segregation-driven intermixing on the thermal transport through planar Si/Ge superlattices," Phys. Rev. Lett. **111**, 115901 (2013).
[27]R. Cheaito, J. C. Duda, T. E. Beechem, K. Hattar, J. F. Ihlefeld, D. L. Medlin, M. A. Rodriguez, M. J. Campion, E. S. Piekos, and P. E. Hopkins, "Experimental investigation of size effects on the thermal conductivity of silicon-germanium alloy thin films," Phys. Rev. Lett. **109**, 195901 (2012).
[28]P. E. Hopkins, "Thermal transport across solid interfaces with nanoscale imperfections: Effects of roughness, disorder, dislocations, and bonding on thermal boundary conductance," ISRN Mech. Eng. 682586 (2013).
[29]P. E. Hopkins, J. C. Duda, C. W. Petz, and J. A. Floro, "Controlling thermal conductance through quantum dot roughening at interfaces," Phys. Rev. B **84**, 035438 (2011).

[30]J. C. Duda and P. E. Hopkins, "Systematically controlling Kapitza conductance via chemical etching," Appl. Phys. Lett. **100**, 111602 (2012).
[31]P. E. Hopkins, L. M. Phinney, J. R. Serrano, and T. E. Beechem, "Effects of surface roughness and oxide layer on the thermal boundary conductance at aluminum/silicon interfaces," Phys. Rev. B **82**, 085307 (2010).
[32]P. E. Hopkins and P. M. Norris, "Thermal boundary conductance response to a change in Cr/Si interfacial properties," Appl. Phys. Lett. **89**, 131909 (2006).
[33]P. E. Hopkins, P. M. Norris, R. J. Stevens, T. Beechem, and S. Graham, "Influence of interfacial mixing on thermal boundary conductance across a chromium/silicon interface," J. Heat Transfer **130**, 062402 (2008).
[34]P. E. Hopkins, J. C. Duda, S. P. Clark, C. P. Hains, T. J. Rotter, L. M. Phinney, and G. Balakrishnan, "Effect of dislocation density on thermal boundary conductance across GaSb/GaAs interfaces," Appl. Phys. Lett. **98**, 161913 (2011).
[35]Z. Su, J. P. Freedman, J. H. Leach, E. A. Preble, R. F. Davis, and J. A. Malen, "The impact of film thickness and substrate surface roughness on the thermal resistance of aluminum nitride nucleation layers," J. Appl. Phys. **113**, 213502 (2013).
[36]Z. Su, L. Huang, F. Liu, J. P. Freedman, L. M. Porter, R. F. Davis, and J. A. Malen, "Layer-by-layer thermal conductivities of the Group III nitride films in blue/green light emitting diodes," Appl. Phys. Lett. **100**, 201106 (2012).
[37]J. P. Freedman, X. Yu, R. F. Davis, A. J. Gellman, and J. A. Malen, "Thermal interface conductance across metal alloy-dielectric interfaces," Phys. Rev. B **93**, 035309 (2016).
[38]B. M. Foley, S. C. Hernández, J. C. Duda, J. T. Robinson, S. G. Walton, and P. E. Hopkins, "Modifying surface energy of graphene via plasma-based chemical functionalization to tune thermal and electrical transport at metal interfaces," Nano Lett. **15**, 4876–4882 (2015).
[39]P. E. Hopkins, M. Baraket, E. V. Barnat, T. E. Beechem, S. P. Kearney, J. C. Duda, J. T. Robinson, and S. G. Walton, "Manipulating thermal conductance at metal-graphene contacts via chemical functionalization," Nano Lett. **12**, 590–595 (2012).
[40]M. D. Losego, M. E. Grady, N. R. Sottos, D. G. Cahill, and P. V. Braun, "Effects of chemical bonding on heat transport across interfaces," Nat. Mater. **11**, 502–506 (2012).
[41]J. Yang, E. Ziade, C. Maragliano, R. Crowder, X. Wang, M. Stefancich, M. Chiesa, A. K. Swan, and A. J. Schmidt, "Thermal conductance imaging of graphene contacts," J. Appl. Phys. **116**, 023515 (2014).
[42]S. Majumdar, J. A. Sierra-Suarez, S. N. Schiffres, W.-L. Ong, C. F. Higgs, A. J. H. McGaughey, and J. A. Malen, "Vibrational mismatch of metal leads controls thermal conductance of self-assembled monolayer junctions," Nano Lett. **15**, 2985–2991 (2015).
[43]Z. Ge, D. G. Cahill, and P. V. Braun, "Thermal conductance of hydrophilic and hydrophobic interfaces," Phys. Rev. Lett. **96**, 186101 (2006).
[44]Z. Tian, A. Marconnet, and G. Chen, "Enhancing solid-liquid interface thermal transport using self-assembled monolayers," Appl. Phys. Lett. **106**, 211602 (2015).
[45]H. Harikrishna, W. A. Ducker, and S. T. Huxtable, "The influence of interface bonding on thermal transport through solid–liquid interfaces," Appl. Phys. Lett. **102**, 251606 (2013).
[46]J. Park, J. Huang, W. Wang, C. J. Murphy, and D. G. Cahill, "Heat transport between Au nanorods, surrounding liquids, and solid supports," J. Phys. Chem. C **116**, 26335–26341 (2012).
[47]K. T. Regner, J. P. Freedman, and J. A. Malen, "Advances in studying phonon mean free path dependent contributions to thermal conductivity," Nanoscale Microscale Thermophys. Eng. **19**, 183–205 (2015).
[48]K. T. Regner, S. Majumdar, and J. A. Malen, "Instrumentation of broadband frequency domain thermoreflectance for measuring thermal conductivity accumulation functions," Rev. Sci. Instrum. **84**, 064901 (2013).
[49]K. T. Regner, D. P. Sellan, Z. Su, C. H. Amon, A. J. H. McGaughey, and J. A. Malen, "Broadband phonon mean free path contributions to thermal conductivity measured using frequency domain thermoreflectance," Nat. Commun. **4**, 1640 (2013).
[50]K. T. Regner, L. C. Wei, and J. A. Malen, "Interpretation of thermoreflectance measurements with a two-temperature model including non-surface heat deposition," J. Appl. Phys. **118**, 235101 (2015).
[51]J. P. Freedman, J. H. Leach, E. A. Preble, Z. Sitar, R. F. Davis, and J. A. Malen, "Universal phonon mean free path spectra in crystalline semiconductors at high temperature," Sci. Rep. **3**, 2963 (2013).
[52]A. J. Minnich, J. A. Johnson, A. J. Schmidt, K. Esfarjani, M. S. Dresselhaus, K. A. Nelson, and G. Chen, "Thermal conductivity spectroscopy technique to measure phonon mean free paths," Phys. Rev. Lett. **107**, 095901 (2011).
[53]K. M. Hoogeboom-Pot, J. N. Hernandez-Charpak, X. Gu, T. D. Frazer, E. H. Anderson, W. Chao, R. W. Falcone, R. Yang, M. M. Murnane, H. C. Kapteyn, and D. Nardi, "A new regime of nanoscale thermal transport: Collective diffusion increases dissipation efficiency," Proc. Natl. Acad. Sci. U. S. A. **112**, 4846–4851 (2015).
[54]M. E. Siemens, Q. Li, R. Yang, K. A. Nelson, E. H. Anderson, M. M. Murnane, and H. C. Kapteyn, "Quasi-ballistic thermal transport from nanoscale interfaces observed using ultrafast coherent soft X-ray beams," Nat. Mater. **9**, 26–30 (2010).
[55]L. Zeng, K. C. Collins, Y. Hu, M. N. Luckyanova, A. A. Maznev, S. Huberman, V. Chiloyan, J. Zhou, X. Huang, K. A. Nelson, and G. Chen, "Measuring phonon mean free path distributions by probing quasiballistic phonon transport in grating nanostructures," Sci. Rep. **5**, 17131 (2015).
[56]J. Yang, C. Maragliano, and A. J. Schmidt, "Thermal property microscopy with frequency domain thermoreflectance," Rev. Sci. Instrum. **84**, 104904 (2013).
[57]X. Zheng, D. G. Cahill, R. Krasnochtchekov, R. S. Averback, and J.-C. Zhao, "High-throughput thermal conductivity measurements of nickel solid solutions and the applicability of the Wiedemann-Franz law," Acta Mater. **55**, 5177–5185 (2007).
[58]E. Lopez-Honorato, C. Chiritescu, P. Xiao, D. G. Cahill, and T. J. Abram, "Thermal conductivity mapping of pyrolytic carbon and silicon carbide coatings on simulated fuel particles by time-domain thermoreflectance," J. Nucl. Mater. **378**, 35–39 (2008).
[59]P. E. Hopkins, "Effects of electron-boundary scattering on changes in thermoreflectance in thin metal films undergoing intraband excitations," J. Appl. Phys. **105**, 093517 (2009).
[60]P. E. Hopkins, "Influence of electron-boundary scattering on thermoreflectance calculations after intra- and interband transitions induced by short-pulsed laser absorption," Phys. Rev. B **81**, 035413 (2010).
[61]P. E. Hopkins, "Thermoreflectance dependence on Fermi surface electron number density perturbations," Appl. Phys. Lett. **96**, 041901 (2010).
[62]Y. Wang, J. Y. Park, Y. K. Koh, and D. G. Cahill, "Thermoreflectance of metal transducers for time-domain thermoreflectance," J. Appl. Phys. **108**, 043507 (2010).
[63]A. N. Smith and P. M. Norris, "Influence of intraband transitions on the electron thermoreflectance response of metals," Appl. Phys. Lett. **78**, 1240–1242 (2001).
[64]H. J. Maris, "Phonon transmission across interfaces and the Kapitza resistance," Phys. Rev. B **19**, 1443–1457 (1979).
[65]C. Thomsen, J. Strait, Z. Vardeny, H. J. Maris, J. Tauc, and J. J. Hauser, "Coherent phonon generation and detection by picosecond light pulses," Phys. Rev. Lett. **53**, 989–992 (1984).
[66]C. Thomsen, H. J. Maris, and J. Tauc, "Picosecond acoustics as a non-destructive tool for the characterization of very thin films," Thin Solid Films **154**, 217–223 (1987).
[67]A. J. Sabbah and D. M. Riffe, "Measurement of silicon surface recombination velocity using ultrafast pump-probe reflectivity," J. Appl. Phys. **88**, 6954–6956 (2000).
[68]A. J. Sabbah and D. M. Riffe, "Femtosecond pump-probe reflectivity study of silicon carrier dynamics," Phys. Rev. B **66**, 165217 (2002).
[69]T. Tanaka, A. Harata, and T. Sawada, "Subpicosecond surface-restricted carrier and thermal dynamics by transient reflectivity measurements," J. Appl. Phys. **82**, 4033–4038 (1997).
[70]E. D. Palik, *Handbook of Optical Constants of Solids* (Academic Press, Orlando, 1985).
[71]H. S. Carslaw and J. C. Jaeger, "Steady periodic temperature in composite slabs," in *Conduction of Heat in Solids*, 2nd ed. (Oxford University Press, 1959), Section 3.7, pp. 109–112.
[72]P. E. Hopkins, J. R. Serrano, L. M. Phinney, S. P. Kearney, T. W. Grasser, and C. T. Harris, "Criteria for cross-plane dominated thermal transport in multilayer thin film systems during modulated laser heating," J. Heat Transfer **132**, 081302 (2010).
[73]A. J. Schmidt, X. Chen, and G. Chen, "Pulse accumulation, radial heat conduction, and anisotropic thermal conductivity in pump-probe transient thermoreflectance," Rev. Sci. Instrum. **79**, 114902 (2008).
[74]A. Feldman, "Algorithm for solutions of the thermal diffusion equation in a stratified medium with a modulated heating source," High Temp. - High Pressures **31**, 293–298 (1999).
[75]A. Giri and P. E. Hopkins, "Transient thermal and nonthermal electron and phonon relaxation after short-pulsed laser heating of metals," J. Appl. Phys. **118**, 215101 (2015).
[76]T. Q. Qiu and C. L. Tien, "Heat transfer mechanisms during short-pulse laser heating of metals," J. Heat Transfer **115**, 835–841 (1993).

[77]R. H. M. Groeneveld, R. Sprik, and A. Lagendijk, "Femtosecond spectroscopy of electron-electron and electron-phonon energy relaxation in Ag and Au," Phys. Rev. B **51**, 11433–11445 (1995).
[78]J. Yang, E. Ziade, and A. J. Schmidt, "Modeling optical absorption for thermoreflectance measurements," J. Appl. Phys. **119**, 095107 (2016).
[79]D. H. Hurley, O. B. Wright, O. Matsuda, and S. L. Shinde, "Time resolved imaging of carrier and thermal transport in silicon," J. Appl. Phys. **107**, 023521 (2010).
[80]M. Khafizov, C. Yablinsky, T. R. Allen, and D. H. Hurley, "Measurement of thermal conductivity in proton irradiated silicon," Nucl. Instrum. Methods Phys. Res., Sect. B **325**, 11–14 (2014).
[81]J. A. Johnson, A. A. Maznev, J. Cuffe, J. K. Eliason, A. J. Minnich, T. Kehoe, C. M. S. Torres, G. Chen, and K. A. Nelson, "Direct measurement of room-temperature nondiffusive thermal transport over micron distances in a silicon membrane," Phys. Rev. Lett. **110**, 025901 (2013).
[82]J. A. Johnson, J. K. Eliason, A. A. Maznev, T. Luo, and K. A. Nelson, "Non-diffusive thermal transport in GaAs at micron length scales," J. Appl. Phys. **118**, 155104 (2015).
[83]H. J. Eichler, F. Massmann, E. Biselli, K. Richter, M. Glotz, L. Konetzke, and X. Yang, "Laser-induced free-carrier and temperature gratings in silicon," Phys. Rev. B **36**, 3247–3253 (1987).
[84]G. L. Eesley, "Generation of nonequlibrium electron and lattice temperatures in copper by picosecond laser pulses," Phys. Rev. B **33**, 2144–2151 (1986).
[85]M. Ghotbi, M. Ebrahim-Zadeh, A. Majchrowski, E. Michalski, and I. V. Kityk, "High-average-power femtosecond pulse generation in the blue using BiB_3O_6," Opt. Lett. **29**, 2530–2532 (2004).
[86]J. Opsal and A. Rosencwaig, "Thermal and plasma wave depth profiling in silicon," Appl. Phys. Lett. **47**, 498–500 (1985).
[87]C. Christofides, I. A. Vitkin, and A. Mandelis, "Photothermal reflectance investigation of processed silicon. I. Room-temperature study of the induced damage and of the annealing kinetics of detects in ion-implanted wafers," J. Appl. Phys. **67**, 2815–2821 (1990).
[88]I. A. Vitkin, C. Christofides, and A. Mandelis, "Photothermal reflectance investigation of processed silicon. II. Signal generation and lattice temperature dependence in ion-implanted and amorphous thin layers," J. Appl. Phys. **67**, 2822–2830 (1990).
[89]D. Guidotti and H. M. van Driel, "Spatially resolved defect mapping in semiconductors using laser-modulated thermoreflectance," Appl. Phys. Lett. **47**, 1336–1338 (1985).
[90]A. Salnick and J. Opsal, "Dynamics of the plasma and thermal waves in surface-modified semiconductors," Rev. Sci. Instrum. **74**, 545–549 (2003).
[91]D. B. Laks, G. F. Neumark, and S. T. Pantelides, "Accurate interband-Auger-recominbation rates in silicon," Phys. Rev. B **42**, 5176–5185 (1990).
[92]U. Strauss, W. W. Ruhle, and K. Kohler, "Auger recombination in intrinsic GaAs," Appl. Phys. Lett. **62**, 55–57 (1993).
[93]B. A. Ruzicka, L. K. Werake, H. Samassekou, and H. Zhao, "Ambipolar diffusion of photoexcited carriers in bulk GaAs," Appl. Phys. Lett. **97**, 262119 (2010).
[94]L. Jastrzebski, J. Lagowski, and H. C. Gatos, "Application of scanning electron microscopy to determination of surface recombination velocity: GaAs," Appl. Phys. Lett. **27**, 537–539 (1975).
[95]D. R. Lide, *CRC Handbook for Chemistry and Physics* (CRC Press/Taylor and Francis, Boca Raton, FL, 2008).
[96]P. J. L. Herve and L. K. J. Vandamme, "Empirical temperature dependence of the refractive index of semiconductors," J. Appl. Phys. **77**, 5476–5477 (1995).
[97]W. S. Capinski, H. J. Maris, T. Ruf, M. Cardona, K. Ploog, and D. S. Katzer, "Thermal-conductivity measurements of GaAs/AlAs superlattices using a picosecond optical pump-and-probe technique," Phys. Rev. B **59**, 8105–8113 (1999).
[98]C. Christofides, F. Diakonos, A. Seas, C. Christou, M. Nestoros, and A. Mandelis, "Two-layer model for photomodulated thermoreflectance of semiconductor wafers," J. Appl. Phys. **80**, 1713–1725 (1996).
[99]Y. Ezzahri, S. Grauby, S. Dilhaire, J. M. Rampnoux, and W. Claeys, "Cross-plan Si/SiGe superlattice acoustic and thermal properties measurement by picosecond ultrasonics," J. Appl. Phys. **101**, 013705 (2007).
[100]R. B. Wilson and D. G. Cahill, "Anisotropic failure of Fourier theory in time-domain thermoreflectance experiments," Nat. Commun. **5**, 5075 (2014).
[101]C. J. Glassbrenner and G. A. Slack, "Thermal conductivity of silicon and germanium from 3 °K to the melting point," Phys. Rev. **134**, A1058–A1069 (1964).
[102]D. E. Aspnes and A. A. Studna, "Dielectric functions and optical parameters of Si, Ge, GaP, GaAs, GaSb, InP, InAs, and InSb from 1.5 to 6.0 eV," Phys. Rev. B **27**, 985–1009 (1983).
[103]A. Othonos, "Probing ultrafast carrier and phonon dynamics in semiconductors," J. Appl. Phys. **83**, 1789–1830 (1998).
[104]J. S. Blakemore, "Semiconducting and other major properties of gallium arsenide," J. Appl. Phys. **53**, R123–R181 (1982).
[105]D.-W. Oh, C. Ko, S. Ramanathan, and D. G. Cahill, "Thermal conductivity and dynamic heat capacity across the metal-insulator transition in thin film VO_2," Appl. Phys. Lett. **96**, 151906 (2010).
[106]V. U. Piesbergen, "Die durchschnittlichen atomwarmen der AIIIBV-halbleiter AlSb, GaAs, GaSb, InP, InAs, InSb und die atomwarme des elements germanium zwischen 12 und 273°K," Z. Naturforsch., A **18**, 141–147 (1963).
[107]R. M. Costescu, M. A. Wall, and D. G. Cahill, "Thermal conductance of epitaxial interfaces," Phys. Rev. B **67**, 054302 (2003).
[108]G. Busch and E. Steigmeier, "Warmeleitfahigkeit, elektrische Leitfahigkeit, Hall-effekt und thermospannung von InSb," Helv. Phys. Acta **34**, 1–28 (1961).
[109]M. G. Holland, "Analysis of lattice thermal conductivity," Phys. Rev. **132**, 2461–2471 (1963).